Operando Raman spectroscopy applying novel fluidized bed micro-reactor technology

Operando Raman spectroscopy applying novel fluidized bed micro-reactor technology

Pablo Beato[1*], Eva Schachtl[2], Katia Barbera[3], Francesca Bonino[3], Silvia Bordiga[3]

[1] Haldor Topsøe A/S, Nymøllevej 55, DK-2800 Lyngby, Denmark

[2] Technische Universität München, Department Chemie, Lichtenbergstr. 4, 85747 München, Germany

[3] Department of Inorganic, Physical and Materials Chemistry, INSTM Centro di Riferimento and NIS Centre of Excellence Universita` di Torino, Via Quarello 11A, 10125 Torino, Italy

*Corresponding author:

Pablo Beato

E-mail: pabb@topsoe.dk

Phone: +4522752000

Fax: +4545272999

Abstract

The concept of a recently developed new fluid-bed micro-reactor technology for spectroscopic purposes is presented. Two case studies where *operando* Raman spectroscopy, has been performed with the new fluid-bed reactor are discussed: investigation of the active phase in a commercial sulfuric acid catalyst (VK38, Haldor Topsøe A/S) and the formation of hydrocarbon molecules in the micropores of zeolites, during methanol to hydrocarbon reaction (MTH). We demonstrate that fluidization of the catalyst particles is absolutely necessary to obtain the real structure of heterogeneous systems under *operando* conditions. The molecular structure of the supported molten phase in the sulfuric acid catalyst is very sensitive to changes in reaction conditions and the correlation with the catalytic data provided interesting new insight, enabling us to establish specific structure-activity relationships. The simultaneous monitoring of reaction products and intermediates in the gas phase and inside the micropores of the catalyst during MTH reaction provides unique details on the shape-selectivity of microporous materials.

Keywords: *Operando* Raman, fluid-bed, sulfuric acid, methanol to hydrocarbons, zeolites.

1. Introduction

Laser Raman spectroscopy is based on the so-called Raman-effect, where monochromatic light interacts with matter, such that photon energy is either transferred to or from matter (inelastic scattering). The difference or shift in energy between the laser excitation and the scattered light is related to rotational, vibrational, phonon- or spin-flip processes in the sample. Due to the usually low Raman cross sections of molecules and solids, high laser powers need to be applied in order to produce a well detectable signal. One inherent problem is therefore the risk of laser-induced damages in the sample. A critical issue, in particular in the field of heterogeneous catalysis, is that laser induced heating may also lead to a significant temperature gradient between the integral catalyst bed and the sampling point [1,2]. However, in the case of *operando* Raman spectroscopy, it is very important to know exactly the temperature at which chemical transformations occur. In both cases – laser heating or laser damage – the final goal of *operando* spectroscopy, namely to establish some kind of structure-reactivity relationship, will be impossible.

It might therefore not surprise that researchers in the field of heterogeneous catalysis have attempted to design special experimental set-ups to circumvent laser induced heating and damages, while still using high laser powers. One possibility to avoid laser heating is to reduce the contact time between the laser spot and the sample by either moving the solid catalyst or the laser beam in a continuous mode. Several complicated, semi-successful ways of reducing the contact time between the laser spot and the catalyst particles inside a micro-reactor can be found in the literature [3-5].

We have recently discovered and developed a new technology to homogeneously fluidize particles inside a micro-reactor and conduct heterogeneous catalytic reactions with it, such that they can be monitored by *operando* Raman spectroscopy, without the drawback of laser heating or damage.

In the following we will illustrate the concept presenting results of two relevant case studies that have been performed with the new fluid-bed reactor:

Case A. Investigation of the active phase in a commercial sulfuric acid catalyst (VK38, Haldor Topsøe A/S) under realistic operation conditions (1 bar, 300 – 630 °C, 10% SO_2, 10% O_2, 80% N_2).

Case B. Follow the formation of hydrocarbon molecules in the micropores of zeolites, during methanol to hydrocarbon reaction (MTH).

2. Experimental

For the experiments on the sulfuric acid catalyst, a Horriba Jobin Yvon LabRam HR confocal microscope equipped with an Ar^+ laser, operated at 514 nm was used. The power at the focal point of a 10x objective was measured to be 12 mW. The slit was opened to 200 µm, and in order to avoid intenisty losses, the confocal hole set to 1100 µm (maximum value). Spectra were taken from 150 cm^{-1} to 1800 cm^{-1}. All *operando* Raman experiments during SO_2 oxidation were performed in the fluidized bed mode in the Linkam CCR1000 reactor. Freshly calcined Daisy-shaped VK-38 catalyst pellets were crushed and between 50 - 55 mg of the sieve fraction from 150 - 300 µm were loaded in the reactor. The feed gas composition was 10 % SO_2, 10 % O_2 and 80 % N_2. The conversion of SO_2 during reaction was measured by a calibrated online IR analyser which detects SO_2 in the exit gas flow (*Figure S1*).

For the zeolite catalyzed methanol to hydrocarbons reaction, Raman spectra were obtained by using a Renishaw micro-Raman System 1000 equipped with an Ar^+ laser (Coherent), frequency doubled to 244 nm. A 15x microscope objective was used for excitation and collection of Raman signal. The laser power at the sample was fixed to ca. 5 mW. The scattered photons were dispersed over a 3600 lines/mm grating monochromator and simultaneously collected on a CCD camera.

Zeolite samples (150 – 300 µm sieve fraction), a ZSM-5 (Si/Al = 50) and a ZSM-22 (Si/Al = 35) have been activated and tested following a common procedure: 1) heating up to 550°C in air stream (20 ml/min); 2) cooling down at the chosen reaction temperature in air stream; 3) switching to He stream (20 ml/min); 4) sequence of three CH_3OH pulses (each of them of 10 sec) by bubbling He (20 ml/min)

through methanol kept at 0°C; 5) long CH_3OH pulse (approx. 5 min); 6) switching back to pure He stream. The reaction products were followed semi-quantitative by online mass spectrometry (*Figure S2*).

3. Reactor concept

A fluidized bed is generated when solid particles present in a vessel are placed at appropriate conditions to cause the solid–gas mixture to behave as a fluid. This is usually achieved by the introduction of pressurized gas through the particulate medium. Fluidized beds are used in many different applications, such as fluidized bed reactors or fluidized bed combustions and are generally characterized by improved heat and/or mass transfer [6].

The reactor used in this study is a modified version of the commercial CCR1000 catalyst cell from Linkam Scientific Instruments (Figure 1a). The reaction gas is flowing downwards from top to bottom of the reactor, passing through the sample, which is supported in a ceramic sample holder on a ceramic fibre filter. Fluidization is achieved via a micro-device, placed downstream the reactor that provokes pressure oscillations in such a way that the flow direction is reversed in discrete pulses of about 40-100 Hz. The particles are lifted upwards by the reverse flow pulses but the net flow direction is still downwards and thereby ensures that the particles stay in the sample holder (Figure 1b). Due to the particular design of the sample holder and the length and the frequency of the pulses, the particles move homogeneously in a quasi-circular mode (*see also video in the supporting material*).

4. Results and Discussion

4.1. Investigation of the active phase in a commercial sulfuric acid catalyst.

Sulfuric acid is the largest volume chemical in the world with an annual production of about 180 x 10^6 t/year which is used primarily for phosphate fertilizers, petroleum alkylation and ore leaching processes. In a sulfuric acid plant sulfur is combusted with dry air at about 1100 °C to a gas that contains 10-12% SO_2 and 9-11% O_2. The gas is cooled in a steam boiler to 380-440 °C and passed to a

series of fixed bed reactors, where SO_2 is oxidised to SO_3 according to the reversible exothermic reaction:

$$SO_2 + ½O_2 = SO_3 + 99 \text{ kJ/mol.} \qquad (1)$$

Commercial sulfuric acid catalysts are based on V_2O_5 dissolved in alkali-metal pyrosulfates, dispersed on an inactive porous silica support. Under reaction conditions the vanadium sulfates form a melt together with the alkali metals, resulting in a so-called supported liquid phase (SLP) catalyst [7]. The catalytic oxidation of SO_2 takes then place as a homogeneous reaction in a liquid film covering the internal surface of the support material. For over 60 years, the harsh reaction conditions and the fact that the active catalyst phase is present in a melt represented a true challenge for scientists trying to obtain detailed structural models of this complex system. Nevertheless, the joint research efforts of a number of groups from Russia, Greece and Denmark for over more then 20 years provided reasonable evidence to propose the reaction mechanism summarized in the schematic drawing of Figure 2 [8-14].

More recently, Boghosian and co-workers [15] applied for the first time *in-situ* Raman spectroscopy on a model catalyst during SO_2 oxidation. They showed that Raman spectroscopy is well suited to observe the structural changes of the catalyst under operating conditions.

We were interested to find out whether it is possible to detect the proposed structures shown in Figure 2 in a commercial sulphuric acid catalyst, *i.e.* the VK38 catalyst from Haldor Topsøe, under industrial reaction conditions. It is known [16-19] that the activity of the catalyst is extremely sensitive to the formation of the molten phase. On the other hand, the heavily coloured catalyst particles (*see photographs in* Figure 3) absorb readily the laser light (514 nm), and hotspots at the sampling area are likely to occur. To obtain reliable structure-activity correlations all *operando* Raman experiments

during SO_2 oxidation were therefore performed in the fluidized bed mode in the Linkam CCR1000 reactor.

Figure 3a shows the two *operando* Raman spectra recorded while switching the gas in the reactor at 380 °C from air to the reaction mixture, containing 10% SO_2 and 10% O_2 in nitrogen. The elapsed time between the two spectra is less than five minutes and is accompanied by a color change of the catalyst from orange-yellow to dark green (Figure 3b). Interestingly, the Raman spectrum of the catalyst before switching to the reaction mixture resembles some characteristic features of the dimeric $V^{(V)}$ complex drawn in Figure 2, which is supposed to be the active species in the proposed cycle. In particular the two bands at ~860 and 770 cm^{-1}, which are assigned to V-O-S and V-O-V bridging bonds, have been claimed to be the signature of the active catalyst [15]. However, the characteristic bands for $V^{(V)}$-vanadyl bonds are missing in the spectrum, indicating the absence of terminal V=O bonds. This might be explained by the extended polymeric nature of melt in the absence of SO_2 from the gas phase. The Raman spectra and the color change after switching to the reaction mixture reveal a structural transformation from a polymeric vanadate to the well defined molecular structure of the $(VO)_3(SO_4)_5^{4-}$ ion [15,17], implying a reduction of $V^{(V)}$ to $V^{(IV)}$. At this point the conversion of SO_2 is close to zero (*Figure S1*).

A significant jump in activity is first observed when the temperature is raised to 480 °C. The corresponding Raman spectrum is shown in Figure 3c. Again the structural changes can be clearly recognized by Raman spectroscopy and accompanied by a color change of the catalyst from dark green to ocher. The most evident new features in the spectrum of the active catalyst are the appearance of a band centered at 1043 cm^{-1}, characteristic for $V^{(V)}$-vanadyl bonds and a broad and structured band between 940 and 985 cm^{-1}, together with two bands at 665 and 605 cm^{-1}, assigned to the vibrational modes of the SO_4 ligands in different vanadium oxosulfato complexes. Less pronounced, but still evident are the spectral features at around 750 and 860 cm^{-1}, which were also observed in the spectrum in air (Figure 3a). Combining the spectral information according to the literature [15] it is possible to conclude that the active phase of the industrial VK38 catalyst at 480 °C corresponds to a mixture of

predominantly monomeric and to minor extend dimeric vanadium (V) oxosulphate species, which fits well with the proposed structures of Lapina *et al.[14]*, shown in Figure 2.

4.2. The formation of hydrocarbon molecules in the micropores of zeolites, during methanol to hydrocarbon reaction (MTH).

With the development of zeolite science, the structural properties of this class of materials have been thoroughly investigated. Great part of the molecular understanding of zeolites has been obtained from vibrational spectroscopies, such as Infrared (IR) and Raman [20-33]. Raman spectroscopy is able to selectively detect the vibrational modes of particular species in a complex mixture which makes the technique also suitable to be used as *operando* technique. However, particularly in the field of zeolite science, Raman has been used far less than IR spectroscopy and is comparably underdeveloped. This is mainly related to the generally low Raman cross sections, resulting in an unfavorable signal-to-noise ratio and the frequently observed broad fluorescence background, caused by organic inclusions and surface defects in the zeolites [24]. Both, the signal-to-noise ratio and the fluorescence problem can be improved if the laser wavelength is moved from the visible to the UV range [34-36]. In fact, if the excitation wavelength is below 260 nm, the Raman shifts typically appear at shorter wavelengths than fluorescence. However, the price of such a high energy wavelength is that the materials under investigation can undergo decomposition by photo-induced reactions. It has also been reported that UV Raman spectra appear to be more sensitive to the out-of-plane bending and symmetric stretching vibrations of bridging oxygen species (M−O−M), whereas the visible Raman spectra are more sensitive to terminal oxygen vibrations (M=O) [37]. In the present case study, we probe the nature of the organic species formed in two different zeolite topologies during methanol conversion under *operando* conditions, by using our recently developed fluid-bed technique. A great number of different zeolite structures have been tested, but for the sake of brevity, in this contribution only results on ZSM-5 and ZSM-22 will be reported. A more dedicated manuscript to the structural characterization of zeolites during MTH reaction is in preparation.

The great advantage of the experimental set-up is evidenced in Figure 4, where *in situ* UV-Raman spectra (λ=244 nm) of an H-ZSM-5 sample in a methanol stream (10 vol% CH_3OH in He) at RT, with and without movement are reported.

As long as the sample is in movement (gray curve, Fig. 4), the Raman spectrum of methanol, physisorbed at the surface of the zeolite is easily recognizable. Main features are: ν(OH) at 3628 cm^{-1}, ν(CH_3) at 2950 cm^{-1} and 2835 cm^{-1}, δ(CH_3) at 1456 cm^{-1}, ν(CO) at 1028 cm^{-1} and ρ(CH_3) at 1150 cm^{-1}. The part of the spectrum at lower energy (1000-250 cm^{-1}) is the Si-O vibrational fingerprint of the H-ZSM-5 zeolite.

When the movement is stopped, the same laser power causes almost immediately the decomposition of methanol, resulting in a completely changed spectrum with the appearance of only one broad band centered at 1560 cm^{-1} (black curve, Fig. 4). The band has been assigned to coke-like species, which have formed during fast polycondensation and dehydration reactions of methanol induced by the high energy laser irradiation. Optically this coking reaction could also be recognized by a black area (on the white zeolite sample) at the point where the laser spot hits the sample. All spectra during methanol conversion where therefore measured in the fluidized-bed mode.

The zeolite samples have been pre-treated in a stream of synthetic air at 550°C for 1h to remove all pre-adsorbed molecules from the surface. The corresponding Raman spectra are the black curves reported in Figure 5a,c revealing the characteristic Raman modes of the zeolites in this range.

The MTH reaction temperature has been chosen differently for the two zeolites, in order to be able to compare the hydrocarbon pool species with previously published results [28,38,39]. The methanol has been introduced first gradually by means of three small pulses (red curves in part a) and c) of Figure 5 and then by a prolonged dosage (blue curves in part b) and d) of Figure 5). The reaction products were followed semi-quantitatively by online mass spectrometry (*Figure S2*). Finally, the methanol feed was stopped and the whole reactor flushed in a He stream (20 ml/min), in order to remove weakly adsorbed species formed upon methanol reaction (green curves in part b) and d) of Figure 5).

In the carbon dedicated literature, the two very intense and broad bands centered at 1600 and 1350 cm^{-1} have been attributed to different forms of sp^2-bonded carbons with various degrees of graphitic ordering, ranging from microcrystalline graphite to glassy carbon [40-51]. In more detail, the higher frequency mode, called "G" peak, involves the in-plane bond-stretching motion of pairs of sp^2 C atoms. This mode does not require the presence of six fold rings, as it occurs at all sp^2 sites, not only those of the rings. It always lies in the range 1500-1690 cm^{-1} and its exact position depends on the degree of order of the sp^2 carbons. In graphitic (ring) systems the band is never observed at positions higher then 1600 cm^{-1}, while for chain type sp^2 carbons with very strained or short isolated C=C bonds it can reach 1690 cm^{-1} (*e.g.* ethylene ~1630 cm^{-1}). On the other hand, the lower frequency mode, called "D" peak, is forbidden in perfect graphite and only appears in presence of disorder. It varies with photon excitation energy, and its intensity is strictly connected to the six fold aromatic rings.

Ferrari et al. showed that by using a laser line in the deep UV range (λ=244nm), the intensity of D peak should be negligible, both in amorphous and graphitic carbon [40,41]. The broad and intense band centered at about 1380 cm^{-1} which is clearly observed in Figure 5, in particular for the longer methanol pulses, must be therefore due to the superimposition of the vibrational modes of aromatic ring-molecules, rather than larger extended structures. As a consequence, the usage of the terms "G" and "D" peak is not correct, when discussing the spectral features of the spectra at this stage.

Let us now review the spectra of Figure 5 in some more detail. In the case of ZSM-5, right from the first pulse, a band at 1602 cm^{-1} starts to grow. Upon the second and third pulses, two more bands at 1376 and 1225 cm^{-1} start to grow. At the same time the intensity of the bands related to the framework vibrations of ZSM-5 is strongly reduced. It is clear that during this phase the hydrocarbon molecules start to build up in the pores of the zeolite. The fact that the band at 1602 cm^{-1} starts to grow first, could indicate that some non-cyclic olefins (*e.g.* butadienes or pentradienes, *etc.*) adsorb initially and are transformed subsequently into aromatic molecules via cyclization reactions. During the long methanol pulse the band at 1361 cm^{-1}, together with a should at higher frequencies is growing significantly and gets even stronger than the 1606 cm^{-1} band. In addition a number of well defined

bands of lower intensity develop (1289, 1225, 1077, 714, 664 and 570 cm^{-1}). This strong increase of the band at 1361 cm^{-1}, characteristic for the aromatic breathing mode of benzenes, together with the characteristic bands at lower frequencies indicates that at this stage the zeolite is filled up with polymethylated benzenes and naphtenes. However, most of these species are not strongly bound to the zeolite surface and are small enough to desorb again, which is demonstrated by flushing with He (still at reaction temperature). The intensity of the band at 1365 cm^{-1} and the bands between 1300 - 550 cm^{-1} is halved after the flush with inert. At the same time the higher frequency shoulder has developed into a band at 1419 cm^{-1}, indicating that this band is related to some polycondensed aromatics, which are trapped in the zeolite pores.

For ZSM-22 the picture looks generally similar, but some striking differences can be observed. Again, the band at 1606 cm^{-1} starts to grow first, but during the subsequent pulses the band at 1390 cm^{-1} does not grow to the same extent as for ZSM-5, pointing to a lower content of aromatic ring molecules. This assumption is confirmed during the long methanol pulse, where the band at 1390 cm^{-1} is growing, but much less compared to ZSM-5. The higher frequency shoulder is absent in the case of ZSM-22, supporting the assumption that this band is related to larger molecules, which do not fit into the more space restricted 1-D structure of ZSM-22. Conversely, for ZSM-22 the flushing with He at 420 °C does not decrease the band at 1390 cm^{-1}. Instead, the spectrum gets better resolved and bands below 1300 cm^{-1} are clearly recognized. For ZSM-22 the aromatics seem to be entrapped in the zeolite and are not able to desorb, but are transformed to thermodynamically more stable aromatic structures.

5. Conclusions

We demonstrate in two examples that fluidization of the catalyst particles is absolutely necessary to obtain the real structure of heterogeneous systems under *operando* conditions. The molecular structure of the supported molten phase in the sulfuric acid catalyst is very sensitive to changes in reaction conditions and the correlation with the catalytic data provided interesting new insight, enabling us to

establish specific structure-activity relationships. The simultaneous monitoring of reaction products and intermediates in the gas phase and inside the micropores of the catalyst during MTH reaction provides unique details on the shape-selectivity of microporous materials. We are currently further developing the experimental set-up to extend the technique for combined *operando* UV-vis/IR/Raman spectroscopy.

References

[1] F.C. Meunier, Chem. Soc. Rev. 39 (2010) 4602-4614.

[2] S.J. Tinnemans, M.H.F. Kox, M.W. Sletering, T.A. Nijhuis, T. Visser, and B.M. Weckhuysen, Phys. Chem. Chem. Phys. 8 (2006) 2413-2420.

[3] W. Kiefer and H.J. Bernstein, Appl. Spectrosc. 25 (1971) 609-613.

[4] A. Müller and T. Weber, Appl. Catal. 77 (1991) 243-250.

[5] Y.T. Chua and P.C. Stair, J. Catal. 196 (2000) 66-72.

[6] Clayton T.Crowe, John D.Schwarzkopf, Martin Sommerfeld, and Yutaka Tsuji, Multiphase Flows With Droplets and Particles, CRC Press, 2011.

[7] J. Villadsen and H. Livejerg, Catal. Rev. -Sci. Eng. 17 (1978) 203-272.

[8] N.H. Hansen, R. Fehrmann, and N.J. Bjerrum, Inorg. Chem. 21 (1982) 744-752.

[9] R. Fehrmann, N.H. Hansen, and N.J. Bjerrum, Inorg. Chem. 22 (1983) 4009-4014.

[10] R. Fehrmann, B. Krebs, G.N. Papatheodorou, R.W. Berg, and N.J. Bjerrum, Inorg. Chem. 25 (1986) 1571-1577.

[11] S.G. Masters, K.M. Eriksen, and R. Fehrmann, J. Mol. Catal. A Chem. 120 (1997) 227-233.

[12] S.B. Rasmussen, S. Boghosian, K. Nielsen, K.M. Eriksen, and R. Fehrmann, Inorg. Chem. 43 (2004) 3697-3701.

[13] G.E. Folkmann, K.M. Eriksen, R. Fehrmann, M. Gaune-Escard, G. Hatem, O.B. Lapina, and V. Terskikh, J. Phys. Chem. B 102 (1998) 24-28.

[14] O.B. Lapina, B.S. Bal'zhinimaev, S. Boghosian, K.M. Eriksen, and R. Fehrmann, Catal. Today 51 (1999) 469-479.

[15] I. Giakoumelou, R.M. Caraba, V.I. Parvulescu, and S. Boghosian, Catal. Lett. 78 (2002) 209-214.

[16] C. Oehlers, R. Fehrmann, S.G. Masters, K.M. Eriksen, D.E. Sheinin, B.S. Bal'zhinimaev, and V.I. Elokhin, Appl. Catal. A. 147 (1996) 127-144.

[17] K.M. Eriksen, D.A. Karydis, S. Boghosian, and R. Fehrmann, J. Catal. 155 (1995) 32-42.

[18] K.M. Eriksen, R. Fehrmann, and N.J. Bjerrum, J. Catal. 132 (1991) 263-265.

[19] S.G. Masters, A. Chrissanthopoulos, K.M. Eriksen, S. Boghosian, and R. Fehrmann, J. Catal. 166 (1997) 16-24.

[20] C.L. Angell, J. Phys. Chem. 77 (1973) 222.

[21] R. Burch, C. Passingham, G.M. Warnes, and D.J. Rawlence, Spectrochim. Acta, Part A 46 (1990) 243-251.

[22] A.J.M. de Man and R.A. van Santen, Zeolites 13 (1992) 269-279.

[23] P.K. Dutta, D.C. Shieh, and M. Puri, Zeolites 8 (1988) 306-309.

[24] P.P. Knops-Gerrits, D.E. De Vos, E.J.P. Feijen, and P.A. Jacobs, Microporous Mater. 8 (1997) 3-17.

[25] A. Miecznikowski and J. Hanuza, Zeolites 7 (1987) 249-254.

[26] Y. Yu, G. Xiong, C. Li, and F.S. Xiao, Microporous Mesoporous Mater. 46 (2001) 23-34.

[27] E. Astorino, J.B. Peri, R.J. Willey, and G. Busca, J. Catal. 157 (1995) 482-500.

[28] K. Barbera, F. Bonino, S. Bordiga, T.V.W. Janssens, and P. Beato, J. Catal. 280 (2011) 196-205.

[29] P. Borges, R. Ramos Pinto, M.A.N.D. Lemos, F. Lemos, J.C. Védrine, E.G. Derouane, and F. Ramôa Ribeiro, J. Mol. Catal. A Chem. 229 (2005) 127-135.

[30] C. Lamberti, E. Groppo, G. Spoto, S. Bordiga, and A. Zecchina, Infrared Spectroscopy of Transient Surface Species, in: C.G.a.H. Bruce (Ed.), Advances in Catalysis, Academic Press, 2007, pp. 1-74.

[31] F. Thibault-Starzyk, I. Stan, S. Abelló, A. Bonilla, K. Thomas, C. Fernandez, J.P. Gilson, and J. Pérez-Ramírez, J. Catal. 264 (2009) 11-14.

[32] N.Y. Topsøe, K. Pedersen, and E.G. Derouane, J. Catal. 70 (1981) 41-52.

[33] A. Zecchina, S. Bordiga, G. Spoto, D. Scarano, G. Petrini, G. Leofanti, M. Padovan, and C.O. Areàn, J. Chem. Soc. , Faraday Trans. 88 (1992) 2959-2969.

[34] Y.T. Chua and P.C. Stair, J. Catal. 213 (2003) 39-46.

[35] C. Li and P.C. Stair, in 11th International Congress on Catalysis 40 th anniversary Studies in Surface Science and Catalysis Vol 101 (J. W. Hightower, W. N. Delgass, E. Iglesia eds.) (1996) 881-890.

[36] P.C. Stair, The Application of UV Raman Spectroscopy for the Characterization of Catalysts and Catalytic Reactions, in: C.G.a.H. Bruce (Ed.), Advances in Catalysis, Academic Press, 2007, pp. 75-98.

[37] Y.T. Chua, P.C. Stair, and I.E. Wachs, J. Phys. Chem. B 105 (2001) 8600-8606.

[38] F. Bleken, W. Skistad, P. Beato, K. Barbera, M. Kustova, S. Bordiga, K.P. Lillerud, S. Svelle, and U. Olsbye, Phys. Chem. Chem. Phys. 13 (2011) 2539-2549.

[39] S. Teketel, P. Beato, U. Olsbye, K.P. Lillerud, and S. Svelle, Microporous Mesoporous Mater. 136 (2010) 33-41.

[40] A.C. Ferrari and J. Robertson, Phys. Rev. B: Condens. Matter 61 (2000) 14095-14107.

[41] A.C. Ferrari and J. Robertson, Phys. Rev. B: Condens. Matter 64 (2001) 754141-7541413.

[42] A. Cuesta, P. Dhamelincourt, J. Laureyns, A. Martínez-Alonso, and J.M.D. Tascón, Carbon 32 (1994) 1523-1532.

[43] J.R. Dennison and M. Holtz, Spectroscopy 11 (1996) 38-46.

[44] M.S. Dresselhaus, G. Dresselhaus, and A. Jorio, J. Phys. Chem. C 111 (2007) 17887-17893.

[45] R. Escribano, J.J. Sloan, N. Siddique, N. Sze, and T. Dudev, Vib. Spectrosc. 26 (2001) 179-186.

[46] E. Liu, X. Shi, B.K. Tay, L.K. Cheah, H.S. Tan, J.R. Shi, and Z. Sun, J. Appl. Phys. 86 (1999) 6078-6083.

[47] M. Nakamizo, R. Kammereck, and J. Walker, Carbon 12 (1974) 259-267.

[48] M.I. Nathan, J. Smith, and K.N. Tu, J. Appl. Phys. 45 (1974) 2370.

[49] E.D. Obraztsova, M. Fujii, S. Hayashi, V.L. Kuznetsov, Y. Butenko, and A.L. Chuvilin, Carbon 36 (1998) 821-826.

[50] Y. Wang, D.C. Alsmeyer, and R.L. McCreery, Chem. Mater. 2 (1990) 557-563.

[51] M. Yoshikawa, G. Katagiri, H. Ishida, A. Ishitani, and T. Akamatsu, J. Appl. Phys. 64 (1988) 6464-6468.

Figure captions

Figures 1. Detailed sketch of the Linkam CCR1000 reactor (a); schematic drawing of the sample holder with flow indications by arrows to illustrate the fluidization principle (b).

Figure 2. Schematic drawing of the proposed reaction mechanism for SO_2 oxidation over an industrial sulfuric acid catalyst (*adapted from [12]*).

Figure 3. *Operando* Raman spectra while switching from synthetic air (a) to SO_2/O_2 (b) at 380 °C and in SO_2/O_2 at 480 °C (c). The photographs to the right of the spectra show the catalyst in the reactor at the respective reaction conditions.

Figure 4. *In situ* Raman spectra of H-ZSM-5 at RT in a methanol stream (10 vol% CH_3OH in He, 20 ml/min) with (gray curve) and without sample movement (black curve). Symbols ** and * indicate N_2 and O_2 gases typically detected when λ_{exc}=244 nm line is used.

Figure 5. *Operando* Raman spectra of ZSM-5 and ZSM-22 during methanol conversion to hydrocarbons (MTH). The black lines in part a) and c) are the Raman spectra after activation in air at 550 °C. The red lines correspond to the spectra after 3 successive pulses of methanol (a,c), and the blue and green lines correspond to the spectra after a long methanol pulse and subsequent flushing with He, respectively (b,d).

Supplementary material to

Operando Raman spectroscopy applying novel fluidized bed micro-reactor technology

Pablo Beato[1*], Katia Barbera[2], Francesca Bonino[2], Silvia Bordiga[2]

[1] Haldor Topsøe A/S, Nymøllevej 55, DK-2800 Lyngby, Denmark

[2] Department of Inorganic, Physical and Materials Chemistry, INSTM Centro di Riferimento and NIS Centre of Excellence Universita` di Torino, Via Quarello 11A, 10125 Torino, Italy

*Corresponding author:
Pablo Beato
E-mail: pabb@topsoe.dk
Phone: +4522752000
Fax: +4545272999

Figure S1. Temperature profile and conversion data for SO_2 oxidation experiment.

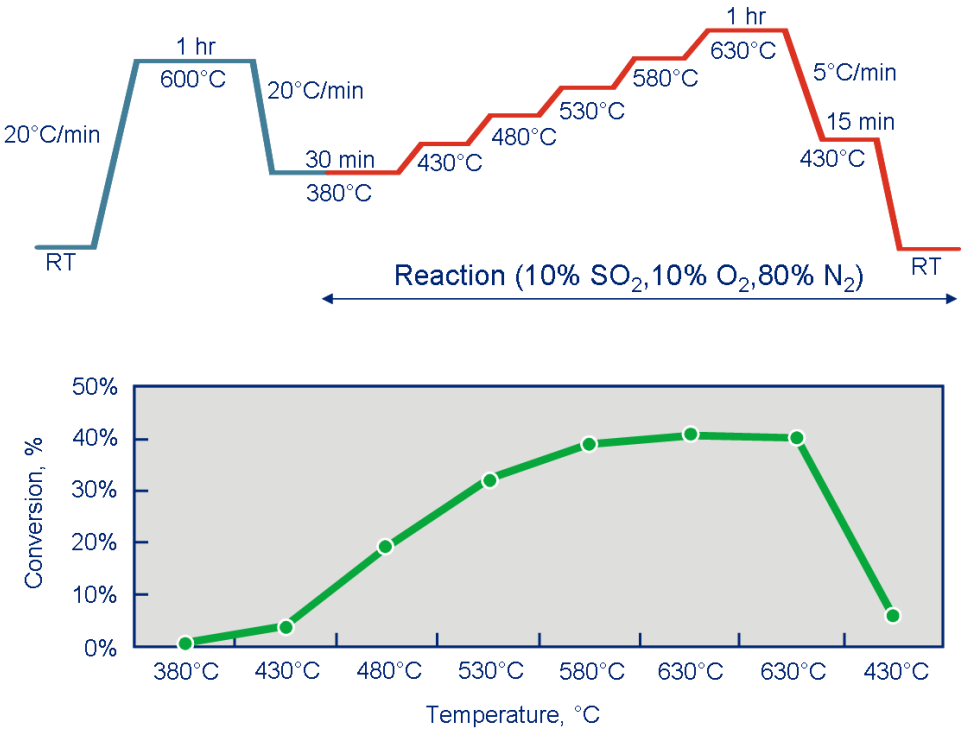

Figure S2. Mass spectrometric data from long methanol pulse (5 min) over H-ZSM-5 and H-ZSM-22.